RESEARCH ARTICLE

Reconstruction and Visualization of 5μm Sectional Coronal Views for Macula Vasculature in OptoVue OCTA

ABDEL-RAZZAK M. AL-HINNAWI [1], **AHMED BANIMUSTAFA** [2], **(Senior Member, IEEE),**
MOTASEM AL-LATAYFEH [3,4], **AND MITRA TAVAKOLI** [5]

[1]Technology of Medical Imaging Department, Faculty of Medical Allied Sciences, Isra University, Queen Alia Airport, Amman 11622, Jordan
[2]Data Science and Artificial Intelligence Department, Faculty of IT, Isra University, Queen Alia Airport, Amman 11622, Jordan
[3]Ophthalmology Department, Prince Hamza Hospital, Amman 11123, Jordan
[4]Faculty of Medicine, Hashemite University, Zarqa 13133, Jordan
[5]Exeter Centre of Excellence for Diabetes Research, National Institute for Health and Care Research (NIHR) Exeter Clinical Research Facility, Institute of Biomedical and Clinical Sciences, University of Exeter Medical School, EX1 2HZ Exeter, U.K.

Corresponding author: Abdel-Razzak M. Al-Hinnawi (abedalrazak.henawai@iu.edu.jo)

ABSTRACT A Computerized Medical Image Processing (CMIP) method is proposed to address the current challenges of optical coherence tomography angiography (OCTA): 1) the need for observing the macula vasculature concerning natural curvature of the macula region; 2) the need for generating OCTA frames at successive small depths in all macula layers; and 3) the need for enhancing the visibility of blood vessels, particularly below the outer retina region. The proposed CMIP method involves image preprocessing, reconstruction, and enhancement stages. Twenty subjects were obtained from the OCTA500 dataset, which was obtained from the OptoVue OCTA machine. The 20 subjects comprise the two OCTA fields of view (FOV), right and left eyes (OD and OS), and five common macula disorders. The sequential enface OCTA images at 5μm macula depths were displayed. The presentation of the macula vasculature was enhanced at all depths. The resulting new ophthalmic views enable: 1) avoiding the superimposition of macula vasculature into a projection map; 2) enhancing the OCTA presentation of blood vessels; and 3) inspecting the macula's 3D oval-shaped. The proposed CMIP method can generate sectional macula coronal views (MCV) for every 5μm depth, clarifying the macula's curvature in a way that has not been presented in OCTA machines. Therefore, "tracking" the 3D propagation of the blood vessel network at all macula depths becomes possible. Furthermore, the blood vessels' display at all macula depths, including the deep choroid layers, is enhanced. The method yields futuristic ophthalmic advantages that would allow the physician to precisely inspect the 3D localization and diffusion of the macula disorders. The method is invariant to the OCTA's FOVs, macula disorder, and OD or OS eye.

INDEX TERMS Computerized medical image processing, optical coherence tomography angiography, macula vasculature, image enhancement.

I. INTRODUCTION

Computerized Medical Image Processing (CMIP) procedures keep advancing [1]. Today, CMIP has ascertained a vital role that helps physicians to determine the healthiness of human anatomical constituents. For example, CMIP procedures allow physicians to inspect the three-dimensional (3D) shape of the human tissues with robust visualization of the junctures between physiological and pathological events, which has efficiently improved the all-around understanding and, thus, the diagnosis of the body parts in all medical imaging systems (e.g. example studies are in references [2], [3], [4], [5]).

In eye imaging, optical coherence tomography (OCT) is a medical imaging technique dedicated to examining the healthiness of the human eye. The OCT device utilizes

The associate editor coordinating the review of this manuscript and approving it for publication was Vishal Srivastava.

LASER radiations to obtain images of the eye's anatomical parts, such as the macula or the optic nerve head [6], [7]. The macula comprises the fovea region and three main sectional layers, the retina, choroid, and sclera. These all exhibit *natural* curvature shape as illustrated in figures in the method section. Macula is the retina's center, responsible for high color-resolution vision (i.e. high acuity). Therefore, any damage to the macula will impair color vision and may cause blindness [8]. For example, Age-related Macular Degeneration (AMD) is one of the common aging diseases that may blur vision due to defects in the macula. The global prevalence of blindness caused by AMD is responsible for about 8.7% of all blindness cases [9], while the global annual incidence of early and late AMD, respectively, is estimated between 0.2% and 1.6% of the cases [10].

Optical coherence tomography angiography (OCTA) is an extension to the OCT device that can be conducted without the need for dye injections. The OCTA utilizes the variations in the OCT signal's amplitude due to blood flow to generate the OCT angiograms (i.e. OCTA images) [11], [40]. For the macula region, the OCTA scan generates projections of the macula's vascular network (i.e. the choriocapillaris and choroid vasculature) at preset depths, permitting the ophthalmologists to diagnose and follow up on different eye diseases in the macula region [11], [12], [13], [14], [40]. Therefore, the research in OCTA is evolving. Despite the OCTA's exceptional clinical advantages, ophthalmologists and OCTA scientists argue that there is still work yet to be done to enhance the display of the macula's blood vessels. The challenge remains to: (1) consider the natural curvature of the macula region; (2) generate successive OCTA views within all distinct macula layers; and (3) enhance the visibility of blood flow at all depths but particularly at the slowest detectable signal drift (i.e. the outer retina and choriocapillaris) [11], [40]. Another OCTA confronts designing algorithms for performing an auto segmentation of the vascular proliferation, producing quantitative parameters, and providing 3D volumetric assessments of choroidal vessels, in addition to reducing image artifacts [11], [15].

The CMIP methods can address some of these OCTA challenges. In literature, many CMIP methods successfully automatically segment the macula's vasculature [16], [17], [18]. These methods cover automatic or semi-automatic segmentation algorithms designed on both the macro and micro macula's vasculature levels. Some researchers suggested extending the OCTA segmentation tasks by producing quantification parameters [17], [19], [20], [41], [42], [43], [44], [45], such as OCTA vessels' length, area density, and diameters. Some studies moved beyond the segmentation and quantitative analysis toward exploring the use of Artificial Intelligence (AI) techniques such as Deep Learning [21], [22], [23], [46], [48] and Machine Learning [24], [47] to classify the delineated vasculature regions into normal or abnormal. These efforts have led to the proposal of computer-aided-detection algorithms for some macula diseases such as Diabetic Retinopathy [24].

Additionally, other researchers investigated the use of 3D volumetric assessment to generate a 3D volume of specified macula's zones (e.g. Fovea Plana) [25], 3D presentation of the entire macula's vessels [26], [27], [49], [50], [51], 3D shape modeling of the macula's microvasculature [28], [52], or 3D metrics of the macula's vessel density [29] and surface [30]. However, considering the 3D shape of the macula, displaying sequential OCTA frames within each macula's layers, and improving the display of vessels at deep regions (i.e. the choroid capillaries), still need addressing.

This paper presents a method to solve these three OCTA challenges. The proposed method utilizes CMIP procedures to reconstruct ''sequential coronal displays'' of the macula. The resulting enface sequential displays would allow physicians to observe blood vessel diffusion at every 5μm successive macula penetrations. Thus, the impact of the macula's 3D curvature shape on the OCTA views can now be visualized. To the best of our knowledge, the OCTA coronal displays have not been presented in the literature. Then, the paper investigates applying a MATLAB function to enhance the display of blood vessels at all macula depths, including the deep retina and choroid capillaries. The applied function allows for selecting and then enhancing the presentation of blood vessels of targeted diameter (micro or macro), which could also help in the OCTA clinic. The method was applied to 20 OCTA scans from the public OCTA500 dataset, which was acquired with two possible OCTA fields of view (FOV) at 3 $\times$ 3mm and 6 $\times$ 6mm from the OptoVue OCTA machine (the RTVue-XR, OptoVue, Canada). The 20 subjects cover the five common macula disorders, OD and OS eyes, and two FOVs. Normal subjects were also considered. The experimental results have shown benefits in ophthalmology, suggesting solutions to the research problems.

II. MATERIALS
A. THE OCT AND OCTA OPHTHALMIC VIEWS
The interference of the reflected and transmitted LASER beams is employed to generate an ophthalmic view in the OCT and OCTA scans [40], as illustrated in equation (1). Both scans display the B-scan of the macula, a series of macula's A-scans (i.e. axial cross-sections) of the main four macula regions: the foveola, fovea, parafovea, and perifovea [6], yielding an ophthalmic 3D view of the macula. The OCT B-scan enables the physicians to examine the macula's structural layers, Internal Limiting Membrane (ILM), Nerve Fiber Layer (NFL), Ganglion cell (GC), Inner Plexiform layer (IPL), Inner Nuclear (IN), Outer Plexiform Layer (OPL), Outer Nuclear (ON), External Limiting Membrane (ELM), Myoid Zone, Ellipsoid zone, Interdigitation Zone, and the Brush Complex (BC) [6], [7]. In contrast, the OCTA B-scan enables ophthalmologists to examine the macula's vasculature [11], [13], [14]. This is achieved by monitoring the variations in the OCT signals of the same A-Scan multiple times to detect the presence of blood flow [12], as seen in equation (2). Then, the OCTA machine generates four

Retina OverVue

Image Type: Angio

Right / OD

3.00 x 3.00 Scan Size (mm)

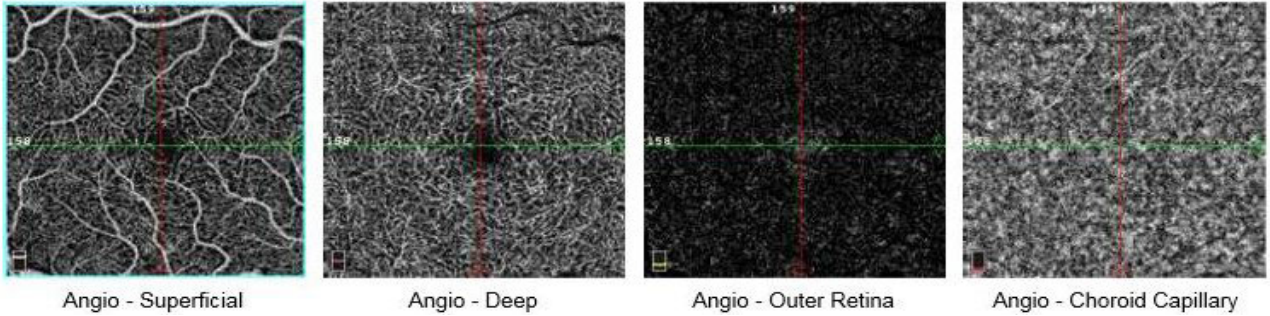Angio - Superficial   Angio - Deep   Angio - Outer Retina   Angio - Choroid Capillary

FIGURE 1. Examples of the four OCTA macula projections obtained from normal OD subject, using the OptoVue OCTA machine.

high-resolution (micron-level) 2D angiograms that demonstrate the projection of the blood vessels proliferation at preset macula's enface depths (i.e. slabs), the superficial capillary plexus, the deep capillary plexus, the outer retina, and the choroid capillaries. Fig. 1 demonstrates example images of these four OCTA macula projection maps from an OD normal subject obtained from the OptoVue OCTA machine.

$$I_D(k) = S(K) = \sum_{n=1}^{N} \sqrt{R_n} R_R (cos\,2Kz_n). \quad (1)$$

where: $I_D(K)$, $S(K)$, K, R_n, R_R, and z_n are the spectral interferogram, the optical power density of the LASER source, modulation frequency, power reflectivity of the sample at position z_n, the reflectivity of reference mirror, depth position, respectively, while n=1 to N is the number of depth positions.

$$Flow\,(x, z) = \frac{1}{N} \sum_{i=1}^{N} (I_i\,(x, z) - I_{mean}). \quad (2)$$

where $I_i(x,z)$ is the intensity value in the i-th A-scan at lateral location "x" and depth position "z", and I_{mean} is the average intensity value over the same set of pixels.

B. OCTA500 DATASET

Li et al. published a dataset of both the OCT and OCTA macula examinations and made it publicly accessible at https://ieee-dataport.org/open-access/octa-500 [32], [33] under the name "OCTA500". The dataset was accessed after receiving permission from the authors. The dataset contains raw macula's ophthalmic 3D volumes showing the OCT and OCTA B-scans for 500 subjects. Two imaging ranges for two FOVs were considered, the 3 × 3×3mm (200 subjects) and the 6 × 6×3mm (300 Subjects). The former was denoted as OCTA-3M, while the latter was denoted as OCTA-6M. The dataset contains both normal and abnormal cases. The abnormal cases include five different macula diseases, Age-related Macular Degeneration (AMD), Choroidal Neovascularization (CNV), Diabetic Retinopathy (DR), Central Serous Chorioretinopathy (CSC), and Retinal Vein Occlusion

TABLE 1. Description of The experimental dataset.

Subject #	OCTA500 case ID	M/F	OD/OS	Age	Disease	FOV
1	10312	M	OD	55	Normal	3 x 3 mm
2	10375	F	OS	58		
3	10458	F	OD	52	AMD	
4	10310	F	OS	55		
5	10474	M	OD	57	CNV	
6	10473	F	OS	35		
7	10384	F	OD	52	DR	
8	10315	M	OS	58		
9	10014	F	OD	56	Normal	6 x 6 mm
10	10016	M	OS	59		
11	10004	M	OD	53	AMD	
12	10079	M	OS	57		
13	10008	F	OD	51	CNV	
14	10274	M	OS	41		
15	10056	F	OD	56	DR	
16	10268	M	OS	57		
17	10070	M	OD	51	CSC	
18	10098	M	OS	47		
19	10299	M	OD	62	RVO	
20	10148	M	OS	54		

(RVO). The OCTA-3M contains the OCT and OCTA B-scans for 200 subjects diagnosed as AMD, CNV, DR, or normal cases. In Comparison, the OCTA-6M contains the OCT and OCTA B-scans for 300 subjects diagnosed as either AMD, CNV, DR, CSC, RVO, or normal cases.

All the subjects were obtained and diagnosed with the RTVue-XR spectral domain OCT machine (the RTVue-XR, OptoVue, Canada), which utilizes a 70KHz LASER beam of 840nm wavelength and a split-spectrum amplitude-decorrelation angiography (SSADA) algorithm to extract the OCTA information. The A-scan rate was 70,000 scans per second. The system's spatial resolution was 5μm and 15μm for the axial and transversal axes, respectively. The A-scan depth was approximated to 3mm. The dataset was generated accordingly to the ethical principles of the Declaration of Helsinki and was approved by the institutional human Subjects Committee [32], [33].

To sustain the results' validity, one OD and one OS subject were randomly selected from each clinical category in the OCTA500. The age of the subjects was in ranged from 50 to
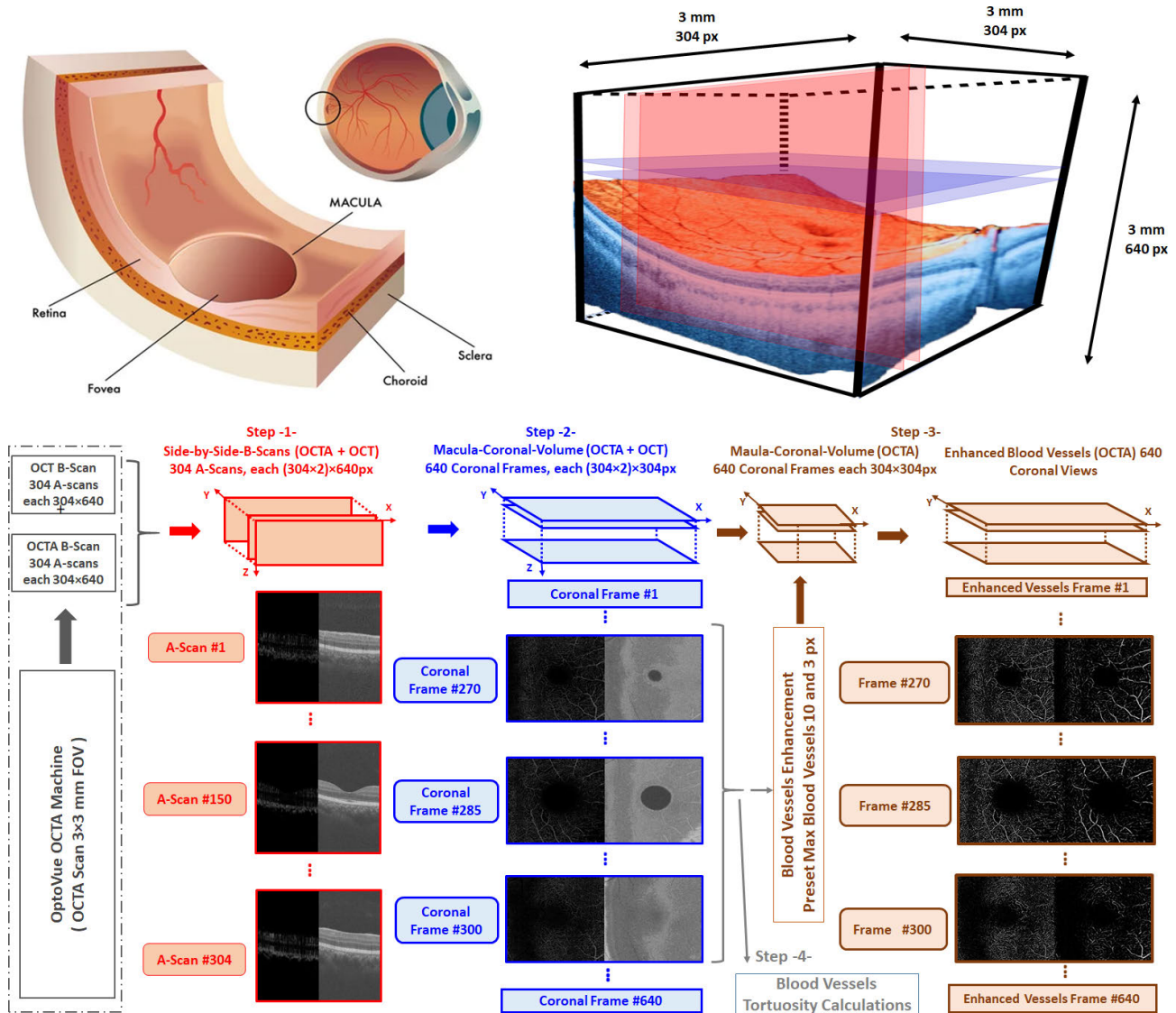
FIGURE 2. The block diagram of the proposed CMIP method.

60 years old. This criterion was employed due to the prevalence of eye diseases in those aged 50 years and more [8], [9]. In case a sample was not found (i.e.50 to 60 years old), the oldest subject in the category was selected. TABLE 1 shows the description of these subjects.

Since the OCTA and OCT scan in the OCTA500 originally has different image resolutions, their volumes were resized using bilinear interpolation, so they all have the same size of $304 \times 304 \times 640$px and $400 \times 400 \times 640$px for both the OCTA-3M and OCTA-6M cases, respectively [32]. This means that each OCTA-3M case consists of 304 macula A-scans, each of which is 304×640px as shown in Fig. 2. Similarly, each OCTA-6M consists of 400 A-scans, each of which is 400×640px. Therefore, the transversal resolution for the OCTA-6M is equal to 15μm (i.e. 6mm/400px), while it is almost 10μm (i.e. 3mm/304px) for the OCTA-3M. Both OCTA-3M and OCTA-6M have the same depth information roughly equal to 5μm (i.e. 3mm/640 px).

III. METHOD

Fig. 2 shows a block diagram illustrating the proposed CMIP method to solve the research problems. The proposed method consists of three steps. The first step is a preparatory step to combine the OCT and OCTA B-Scans. The second CMIP step involves reconstructing OCT and OCTA coronal displays. In contrast, the third CMIP step involves enhancing the appearance of the macula's blood vessels based on their width (i.e. the micro and macro blood vessels). The second step is fully automated without intervention by the user, whereas the third step prompts the user to preset the requested blood vessels' width according to his/her investigation interest.

A. STEP-1- SIDE-BY-SIDE OCTA AND OCT B-SCANS

For each subject in TABLE 1, the $304 \times 304 \times 640$px OCT and OCTA B-scans were concatenated horizontally, yielding side-by-side B-scans. The images in the red frames in Fig. 2 demonstrate examples. The new 3D volume is called

TABLE 2. The 3d dimensions of the 3d volumes of the original and resulting macula vasculature views.

FOV	OCT B-Scan	OCTA B-Scan	Side-by-Side-B-Scans	Macula Coronal Views	Enhanced Macula Vasculature (10px or 3px Max. width)
OCTA-3M	304×304×640	304×304×640	304×608×640	640×608×304	640×608×304
OCTA-6M	400×400×640	400×400×640	400×800×640	640×800×400	640×800×400

"Side-by-Side-B-Scans". It is $304×(304 × 2)×640$px in size for each OCT-3M case and $400×(400 × 2)×640$px in size for each OCT-6M case. TABLE 2 illustrates the size of the 3D volumes before and after applying this preliminary step to all subjects. This step is a preparatory step, but it is essential for the following steps. Section IV provides further explanation. The table also records the size of 3D volumes resulting from the other steps in the proposed CMIP method

B. STEP-2- GENERATION OF THE MACULA'S CORONAL VIEWS

The Side-by-Side-B-scan video was re-sliced from top to bottom. This was performed, so that the original image resolution was retained (i.e. without interpolation). Thus, the orthogonal information at X, Y, and Z information remain unchanged, as seen in Fig.2. Consequently, a Side-by-Side-B-Scans 3D volume that has the size of $304 × 608×640$px becomes a $640 × 608×304$px 3D volume for any OCT-3M case (TABLE 2). Similarly, the macula's coronal volume for any OCTA-6M cases is $640 × 800×400$px (TABLE 2). To the best of our knowledge, this methodology of generating the macula ophthalmic coronal views has not been presented in the literature.

From medical imaging science technology, slicing axial slices from top to bottom should produce coronal views. The images with blue frames in Fig. 2 demonstrate examples of the resulting coronal views. Accordingly, if this step was applied to OCTA B-Scan only, one should be able to display the enface macula's vasculature (i.e. the vasculature coronal views). Whereas, if this step was applied to OCT B-Scan only, one should be able to visualize the coronal views of both the macula histology and the macula vasculatures. The resulting reconstructed video was labeled as the OCT and OCTA "Macula-Coronal-Volume".

C. STEP-3-: IMAGE ENHANCEMENTS OF MACULA BLOOD VESSEL

A MATLAB library contains a function that is called "fibermetric", which can be used to enhance any elongated and tubular structures in an intensity (grey levels) image using Hessian-based multiscale filtering [34], [35], as illustrated in equation (3).

$$H_{ij}(x, s) = s^2 I(x) * \frac{\partial^2}{\partial x_i \partial x_j} G(x, s) \ for \ i, j = 1, \ldots, D.$$

$$(3)$$

where I(x) is the intensity of a D-dimensions image, $H_{ij}(x,s)$ is the Hessian of I(x) at "x" and scale "s", i,j=1 ...D,

and G(x,s) is the D-variate Gaussian while "*" denotes convolution. The eigenvalues λ_{ij} are obtained through the eigenvalue decomposition eigH(x,s) leading to the D×D matrix. Thus, for a 2D image (D=2), a $2×2$ matrix is obtained for each pixel. The elongated structures are enhanced everywhere $|\lambda_2| \gg |\lambda_1|$ happens. Jerman et al proved that this filter outperforms the other seven enhancement functions in three different clinical applications, fundus vasculature, thoracic CT lung vasculature, and X-Ray DSA cerebral vasculature [35]. For fundus images, which is the image of the interior surface of the eye opposite the lens, the filter remarkably highlights the blood vessels [35]. In this paper, the MCVs also contain blood vasculatures as in the fundus images, but at successive macula depths. This processing step aims to explore the application of this filter on the results from the prior step. Therefore, to evaluate the responses, the contrast before and after applying the filter was calculated (equation (4)). A value of one was added to the minimum value in case it was equal to zero.

$$\text{MCVContrast} = \frac{\text{MaxIntnsity}}{\text{MinIntensity}} \qquad (4)$$

The filter is available in the MATLAB library Ver.2019a. It computes the likeliness of an image region to contain ridges in the image. It needs four inputs: the 2D gray image, condition of the required tubular structure thickness, object polarity (Dark objects on a bright background or Bright objects on dark background), and structure sensitivity (threshold to differentiate tubular structure from background). It was applied to OCTA macula coronal volume only. The aim is to enhance the visibility of vessels in all frames. The function has a user-adjustable preset variable that determines the requested tubular structures' thickness, which needs improvement. In this paper, two thicknesses were tested, based on 10px and 3px, as seen in Fig. 2. The former is used to enhance the blood vessels whose maximum width is 100μm (10px$×10\mu$m), while the latter is used to enhance the blood vessels whose maximum width is 30μm (3px$×10\mu$m). These calculations are based on the fact that the Optovue machine exhibits 10μm transversal resolution for $3 × 3$mm FOV. For the $6 × 6$mm FOV, which exhibits a 15μm transversal resolution, the maximum width of the enhanced blood vessels becomes either 150μm (10px$×15\mu$m) or 45μm (3px$×15\mu$m). Therefore, the function was applied twice, once for each requested thickness. The resulting two OCTA macula coronal volumes were concatenated into a single 3D volume presenting the enhanced OCTA macula's blood vessels (the enhanced 3px view is placed on the left while the 10px view is placed on the right). The images in brown frames in Fig. 2 illustrate examples.

TABLE 3. The results supplementary video.

Case #	Step -1-	Step 2 + 3
1	01-Results-Step-1- Normal OD 3M	01-Results-Step-2+3- Normal OD 3M
2	02-Results-Step-1- Normal OS 3M	02-Results-Step-2+3- Normal OS 3M
3	03-Results-Step-1- AMD OD 3M	03-Results-Step-2+3- AMD OD 3M
4	04-Results-Step-1- AMD OS 3M	04-Results-Step-2+3- AMD OS 3M
5	05-Results-Step-1- CNV OD 3M	05-Results-Step-2+3- CNV OD 3M
6	06-Results-Step-1- CNV OS 3M	06-Results-Step-2+3- CNV OS 3M
7	07-Results-Step-1- DR OD 3M	07-Results-Step-2+3- DR OD 3M
8	08-Results-Step-1- DR OS 3M	08-Results-Step-2+3- DR OS 3M
9	09-Results-Step-1- Normal OD 6M	09-Results-Step-2+3- Normal OD 6M
10	10-Results-Step-1- Normal OS 6M	10-Results-Step-2+3- Normal OS 6M
11	11-Results-Step-1- AMD OD 6M	11-Results-Step-2+3- AMD OD 6M
12	12-Results-Step-1- AMD OS 6M	12-Results-Step-2+3- AMD OS 6M
13	13-Results-Step-1- CNV OD 6M	13-Results-Step-2+3- CNV OD 6M
14	14-Results-Step-1- CNV OS 6M	14-Results-Step-2+3- CNV OS 6M
15	15-Results-Step-1- DR OD 6M	15-Results-Step-2+3- DR OD 6M
16	16-Results-Step-1- DR OS 6M	16-Results-Step-2+3- DR OS 6M
17	17-Results-Step-1- CSC OD 6M	17-Results-Step-2+3- CSC OD 6M
18	18-Results-Step-1- CSC OS 6M	18-Results-Step-2+3- CSC OS 6M
19	19-Results-Step-1- RVO OD 6M	19-Results-Step-2+3- RVO OD 6M
20	20-Results-Step-1- RVO OS 6M	20-Results-Step-2+3- RVO OS 6M

D. TORTUOSITY CALCULATION OF MACULA BLOOD VESSELS

Several OCTA quantification metrics can be calculated from OCTA volume such as various vessel density measures (e.g. perfusion density, binarized vessel density or vessel area density, skeletonized vessel density), complexity measures (e.g. vessel tortuosity, fractal dimension, branching point index), and area and shape measurements of specific regions (e.g. the foveal avascular zone or any segmented neovascular lesions) [40]. These metrics imply clinical perspectives in the assessment of disease progression and their documentation in comparison to normal findings [40].

Tortuosity (τ) is a measure that is often used to quantify blood vessels' shape in retina images [41]. In this paper, it was chosen as a representative of other OCTA metrics. The aim was to assess the possibility to calculate the OCTA metrics from the proposed MCVs. Several calculation methods can be used to calculate the vessels' tortuosity [41] such as equation (5), which was implemented by applying three processes to each MCV. First, each MCV is threshold to segment blood vessels. The threshold was set to 5% higher than the background. Then, a skeletonizing function was applied, and all vessels less than 5px were discarded. After that, the average "τ" for all vessels is calculated for each MCV. This was applied to all 640 MCVs in each subject. The code is attached as a supplementary file (MATLAB code -2-).

$$Tortousity = \frac{\sum VesselLength}{\sum Vessel\ Eucledian\ Distance}, \quad (5)$$

E. PROGRAM PLATFORMS

The method was implemented using the ImageJ platform (Step-1 and 2) and the MATLAB platform 2019a (Step -3- and the tortuosity calculations). Two MATLAB codes are added as supplement files. All steps were processed in a personal computer (PC) with the following main specifications: Intel®_Core™ i7-6500U CPU@2.5GHz, 2 Core(s), 4 Logical Processor(s), 64 bits, and 8.00 GB RAM.

IV. RESULTS

The proposed method was applied to all cases in TABLE 1. The experiments generated a set of 640 OCTA coronal frames (3D volume) for steps -2- and -3-, which were described in the methodology section (section III), making them impossible to present in the body of the manuscript. Thus, all the resulting 3D volumes were saved as animation files using the "MP4" and "AVI" video formats. The "MP4" videos were reported in the attached files, while the "AVI" high-resolution videos are available on the IEEE DataPort website: https://dx.doi.org/10.21227/gx1z-tj11 [31]. This was done due to the storage size limit of supplementary videos. TABLE 3 provides a summary of the attached videos (3D volumes) resulting from each step to make referring to these files easier.

The first step was applied as a preparatory step to addressing the research problems. It aims at managing the OCTA and OCT signals to be processed simultaneously but separately. Fig. 3 illustrates a "Still-Frame" from one of the frames in the B-Scan from an AMD OD subject (case No. 3). Two advantages are achieved by this step. First, the OCTA signals (i.e. macula vasculature signals) are isolated from the influence of the adjacent OCT signals (i.e. macula constant tissue signals) in all A-scans. Second, the OCTA signals are not superimposed on OCT signals. Thus, this would improve the success of any next image processing step. Twenty video files are attached as supplements to show the resulting side-by-side OCT and OCTA B-scans of all subjects. In TABLE 3, they
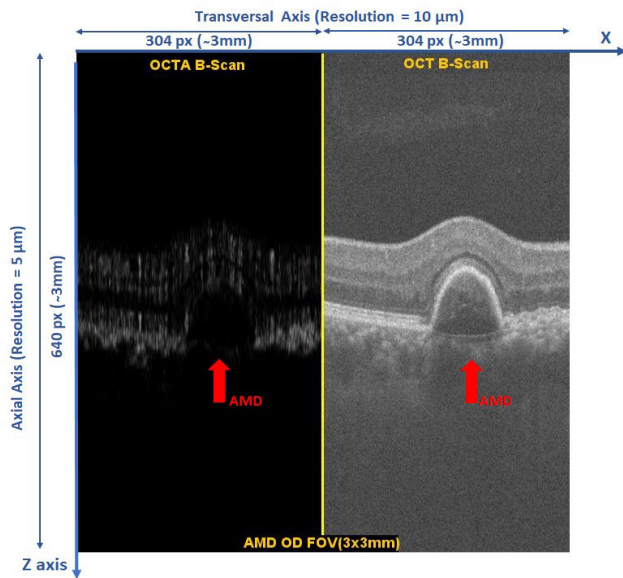
FIGURE 3. A Still-Frame of the Side-by-Side OCTA and OCT B-Scans for an AMD case (Subject #3) with image resolutions.
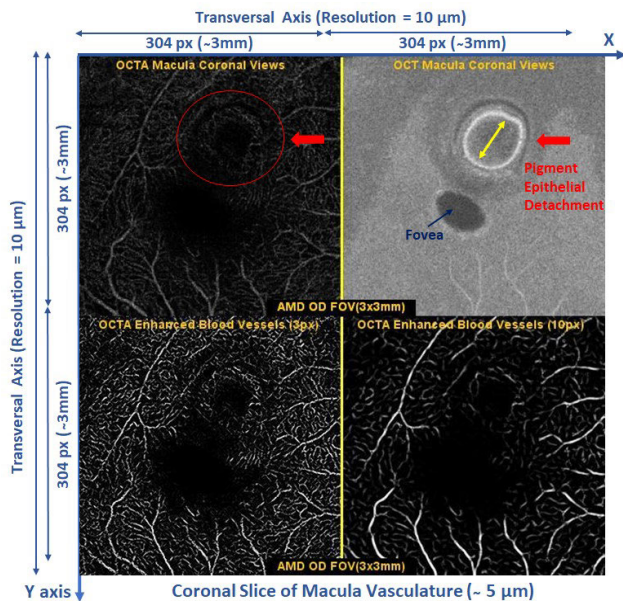

FIGURE 4. A Still-Frame of the resulting MCV from Step-2 (top images) and the Enhanced MCV (3 and 10 px) from Step-3- (Subject #3).

are denoted with the string ''Results-Step-1-'' followed by the word ''diagnosis'', OD or OS, and the ''size'' of the FOV. The video files were organized based on the case number in TABLE 1. Thus, a corresponding number is added at the start of the file name.

The second step was applied to all the Side-by-Side-B-Scans 3D volumes to generate a ''Macula-Coronal-Volume''. This step resulted in OCT and OCTA coronal frames at all depths of the macula's structures, yielding 640 frames for each case. Thus, this step displays the sectional coronal macula vasculature through the macula layers' depths: ILM, NFL, GC, IPL, IN, OPL, ON, ELM, and BC. According to medical imaging science, the signals (i.e. information) at the X, Y,

and Z coordinates remain unchanged in all orthogonal views (i.e. sagittal, axial, and coronal) of any 3D medical imaging examination. Thus, the Z-coordinate in the OCT and OCTA B-Scans, which is the axial depth information, becomes the slice thickness of all coronal views, as demonstrated in Fig. 2. Therefore, the resulting slice thickness for each MCV is equal to the axial resolution of the OCTA machine, which is 5μm in the OptoVue OCTA device (Fig. 3). Fig. 4 illustrates a ''Still-Frame'' of an MCV from the OCTA and OCT MCVs for the same AMD case (subject #3) in Fig. 3. The upper two images in Fig. 4 show the resulting MCV after applying step -2-. The bottom two images show the enhanced MCV of applying step-3-, as will be explained later in the following sections.

The results of applying Step-2- to all subjects in TABLE 1 are included in the supplementary videos as it is impractical to present the 640 frames for each subject in the main text. These are labeled with the string 'Result-Step-2+3-' at the beginning of the name of each file, as illustrated in TABLE 3. The videos were organized to match their number in TABLE 1 (e.g. the file name ''08-Results-Step-2+3'' corresponds to subject No. ''08''). It is important to note that the regions in the front of and behind the macula do not give OCTA signals and thus appear black. Therefore, the onset and the ending of the MCVs show tens of images appearing as black, as can be noticed in all videos resulting from applying step-2- and step-3-.

In step 3, the vessel enhancement function was applied to the OCTA MCVs only, as shown in Fig. 2. This step was applied twice at 10px and 3px, as explained in the method. The step resulted in generating two 3D volumes, each of which is $640 \times 304 \times 304$px in size (see TABLE 2). The first 3D volume demonstrates the enhancement of vessels whose maximum width is 10px (bottom-right of Fig 4), while the second 3D volume shows the enhancement of vessels whose maximum width is 3px (bottom-left of Fig 4). The applied MATLAB function succeeded in suppressing the regions associated with the macula's structures while highlighting the appearance of the macula's blood vessels. This happened at various depths including the deep regions (i.e. the outer retina and the choroid capillaries). The resulting two 3D volumes were concatenated side by side, yielding a 3D volume of $640 \times (304 \times 2) \times 304$px (TABLE 2). This 3D OCTA volume was called ''Enhanced Blood Vessels''. Thus, another 20 video files were generated to demonstrate the results from all 20 subjects. They were concatenated to the 3D volumes resulting from applying step -2- so that both results from step-2- and step-3- appear in one animation video, as shown in Fig 4. Each video shows the 640 MCVs for each subject before and after applying the enhancement step. The contrast for each MCV on all subjects was calculated. Fig. 5 plots the average contrast values for the same MCV of all subjects before and after applying the enhancement filter. It illustrates that there is approximately up to two folds gain in the MCVs' contrast after applying the enhancement filter.

Finally, the skeletonizing step was applied to all 640 OCTA MCVs in each subject. Fig. 6 illustrates an example of
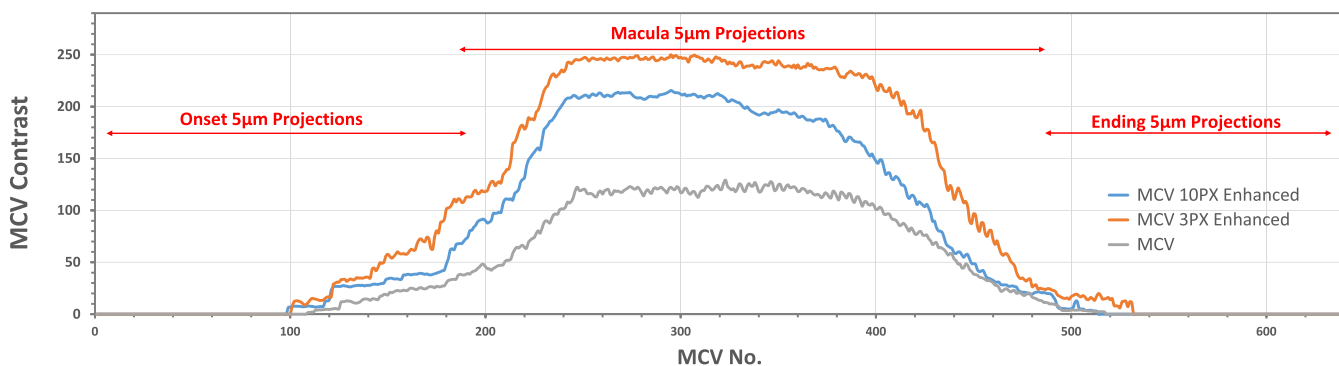
FIGURE 5. Chart of the average contrast in all MCVs for all subjects before and after applying the 3px and 10px enhancement filter (Step -3-).
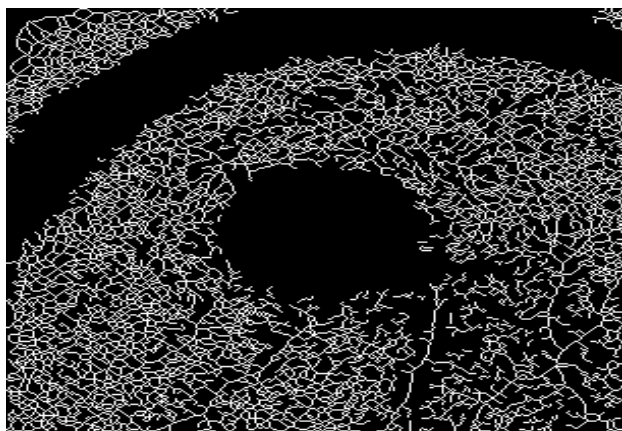

FIGURE 6. Example of the Blood vessels skeleton after segmenting and skeletonizing the MCV (Subject #6, MCV #288).

the resulting blood vessel skeleton in one of the MCVs. Then, the average tortuosity of all vessels present in each MCV is calculated for all subjects, as illustrated in the supplementary EXCEL file. Fig. 7 plots a chart showing the average tortuosity value for all MCVs of all subjects.

V. DISCUSSION

This paper continues the ongoing research in this field which aims to employ CMIP procedures that generate new ophthalmic 3D visualizations from OCT machines [36], [37], [38]. The proposed method in Fig. 2 includes three CMIP steps to solve some of the current OCTA challenges and limitations [11], [12], [13], [14], [15]. The preparatory first step is to put the OCT and OCTA B-scans side by side, as seen in Fig. 3. This step permits assessing the outcome of applying CMIP on OCTA and OCT signals separately. The second step reconstructs 5μm sectional MCVs visualizing the macula vasculature 3D propagation, as seen in the supplementary videos. Thus, this step permits depicting the macula vasculature at consecutive (i.e. successive slice thickness) enface macula depths. This could offer significant importance as it enables physicians to examine the 3D blood flow in the vessels at every 5μm depth (the OCTA machine's axial resolution). Therefore, three important findings can be concluded. First, the ophthalmologists can now monitor each 5μm distinct macula's sequential sections. Second, the 3D diffusion of the macula defect can be observed. Third, the 3D curvature nature of the macula region becomes noticeable and inspectable. Consequently, the sectional MCVs should help physicians determine the *precise* transversal and axial location of macula's vasculature disorder if occurs. In other words, the 3D diffusion of macula vasculature can be monitored. Therefore, it is rational to conclude that the sectional MCVs *present a suggested solution for the first two research problems* (i.e. the need to consider the natural arch of the macula in the OCTA display, and the need to display the OCTA successive individual sections in the macula's layers). This is the major contribution of this paper. It permits ''3D tracking'' of the spreading of macula vasculature at 5μm sequential axial depths.

On the other hand, step-3 helps enhance the appearance of the vessels in the MCVs. This step is user-dependent and can be performed based on the required blood vessel widths that the examiner can preset. In this work, the blood vessels of widths ranging from 30 to 100μm were assessed for OCTA-3M and from 45 to 150μm for OCTA-6M. The results were profitable on all MCVs resulting from the previous step for all subjects, as shown in Fig. 4 and the supplementary videos. This step highlighted the blood vessels' appearance at all macula depths, including those in the outer retina and BM. Fig. 5 demonstrates that this enhancement filter yields gain in enhancing the contrast of the 3px and 10px blood vessels. Although there is more enhancement in 3px than the 10px vessels, this could still aid physicians in the diagnosis process at the OCTA clinic. Other vessels, that are 3px to 10px in diameter, will also be enhanced. Thus, this paper's second contribution is that applying the suggested MATLAB function to MCVs could provide a *solution for the third research challenge* (i.e. the need to improve/enhance the display of the blood vessels at the deep macula layers). It is important to emphasize that this step is not a segmentation of blood vessels. However, it can still be used as an effective method for preprocessing before any segmentation steps that could be conducted later, such as thresholding [16], [17], [18].
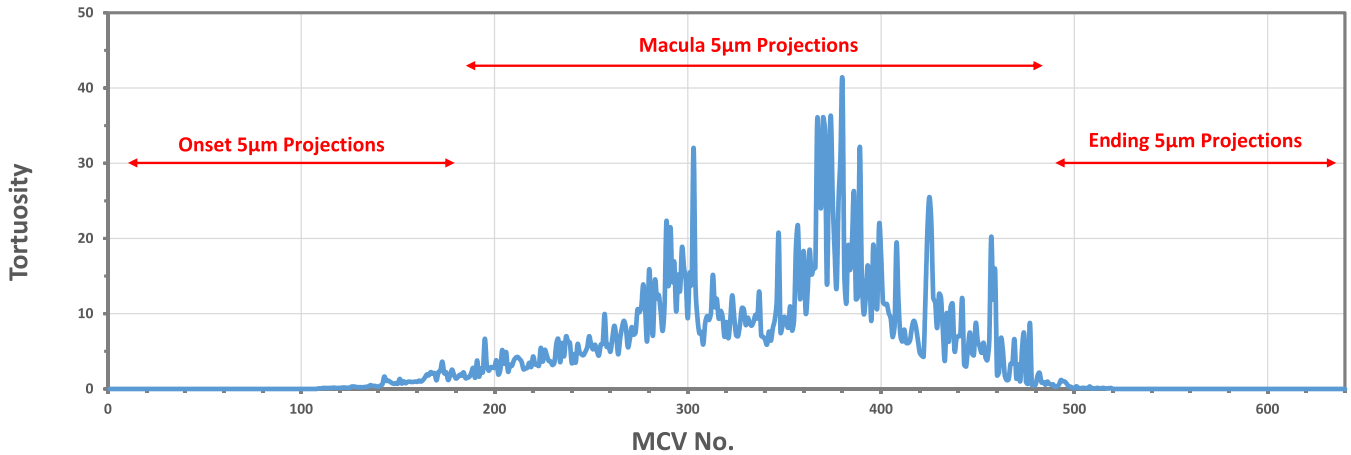
FIGURE 7. Chart of the average tortuosity in all MCVs for all subjects.

Furthermore, the 640 MCVs have a potential consequence advantage. It should allow the physician (or the OCTA device preset panel) to generate projections at any depth. Fig. 8 and Fig. 9 show an example where the first 220 MCVs and the last 180 MCVs were averaged in terms of their intensity to display the "black" regions in front of and behind the macula (i.e. no OCTA signal), while every 10 MCVs in the remaining 240 MCVs were also averaged in terms of their intensity to show projections of macula slabs. Since each MCV shows a 5μm slice thickness (Section III), each macula projection in Fig. 8 and 9 displays vessels in 50μm macula thickness (10 × 5μm=50μm thickness). In Comparison, the onset and end projections display 1100μm (220 × 5μm=1100μm) and 900μm (180 × 5μm=900μm), respectively. Fig. 8 and 9 are also attached as supplement files illustrating the full-scale images for further clarification. It is important to remark that the physician may apply average intensity of less or more than 10 MCVs. Therefore, those two figures demonstrate a *futuristic advantage* in Comparison to Fig. 1. The images in Fig. 1, which were also obtained from the OptoVue OCTA machine, are the standard projections of several tens of microns of macula thickness. Thus, the depth of information is lost. For example, if a macula disorder was to happen at a deep location, then it may either be hidden by the above and lower healthy macula, or it may not be easily perceived. On the contrary, the method in this paper permits the accumulation of any number of MCVs, which sustains the significance and applicability of the proposed CMIP method.

From a technical point of view, all the subjects in TABLE 1 was obtained from an OptoVue OCTA machine that employs an 840nm LASER beam, SSADA algorithm, 70,000 A-scans per second, axial resolution of 5μm, transversal resolution of 10 or 15μm, and A-scan depth of ∼3mm. Although all the latter factors impact the quality of the OCTA images from different vendors [39], the proposed method utilizes straightforward CMIP procedures independent of these factors. The method is anticipated to operate correctly on other OCTA machines manufactured by other vendors as far as the OCTA examination is feasible (e.g. Topcon or Heidelberg). Furthermore, if the OCTA signal resolution were improved by one mean or another, as requested in the references [6], [7], [11], [12], [13], [14], [15], the results of the CMIP method would be expected to become even more apparent. This is future research that would emphasize the robustness of the method.

From a patient point of view, the results were independent of OCTA FOV and patients' anthropometric characteristics such as age, sex, or whether it is applied to the right or left eye of the patient. The method is anticipated to work consistently if the OCT/OCTA B-Scans is feasible. This sustains the robustness of the method.

Clinically, the proposed method was applied to subjects with five different common macula diseases (TABLE 1). Local and international expert physicians (third and fourth coauthors) revised the results from all subjects. They reported that the proposed CMIP procedures presented *futuristic* new ophthalmic visualization of successive 5μm sectional MCVs of any OCTA exam. Not only would the 5μm sequential enface MCVs help to diagnose the 3D diffusion of the macula defects, but it could reveal further findings that may be missed. For instance, in one of the AMD cases (Subject #3), the physicians noticed the presence of a huge retinal pigment epithelium (RPE) detachment, as seen in Fig. 10, pinpointing an abnormal retinal vasculature lesion. In another AMD case (Subject #4), the physicians also noticed the presence of a choroidal neovascular (CNV) membrane lesion, as seen in Fig. 11. Additionally, in one of the DR cases (Subject #7), they noticed the presence of an irregular foveal avascular zone (FAZ) and an area of no perfusion, as seen in Fig. 12. A possible other macula disorders were also noticed in the RVO and CSC cases (subjects #17-20). For all subjects, the ophthalmologists claimed that the methodology could help determine the disease's precise axial and transversal 3D location and 3D size. They argued that this could be *a futuristic advantage and benefit* in OCTA clinics (detection and

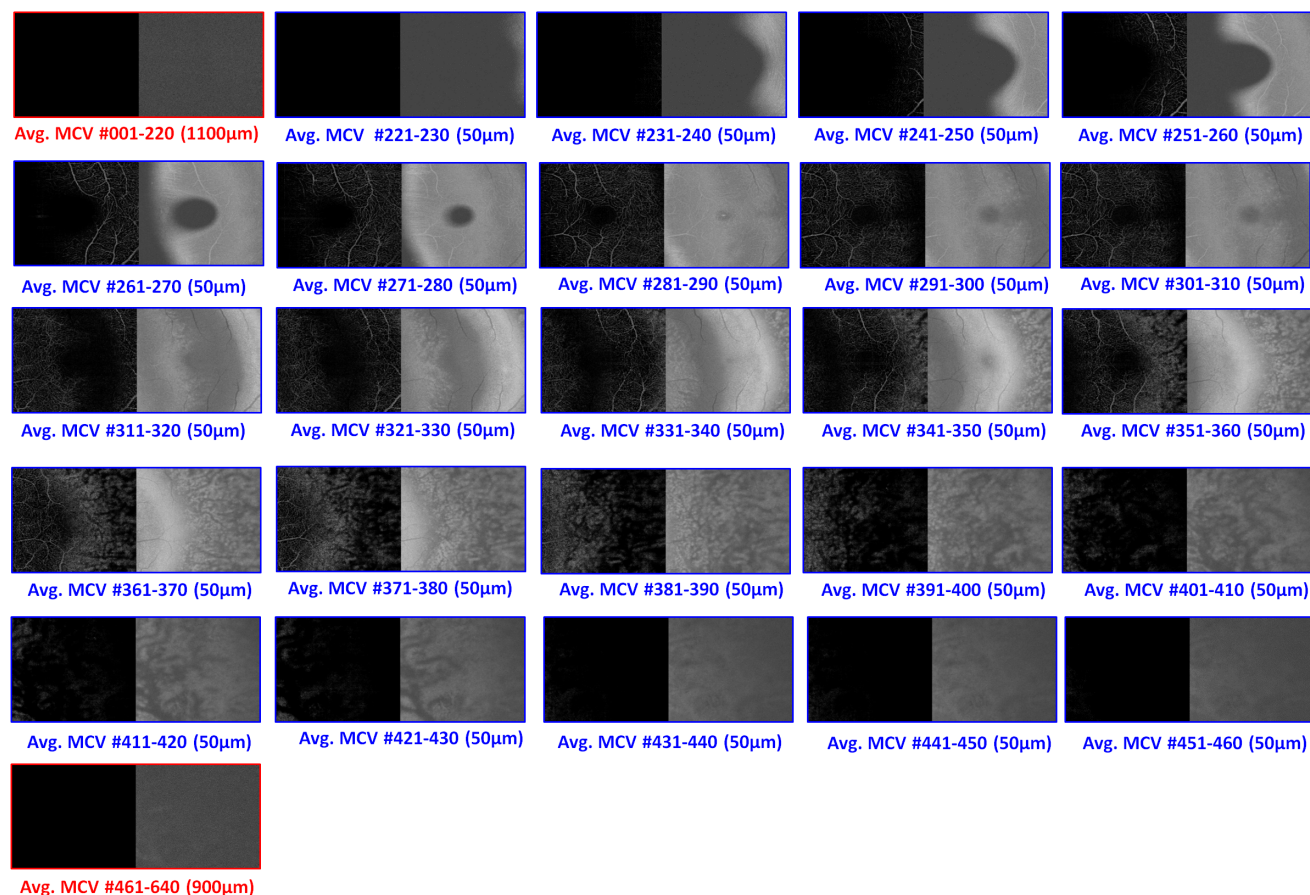## OCTA Macula Coronal Views (MCV)

FIGURE 8. The projections of average MCVs from OCT and OCTS B-scans after applying Step-2-. The average intensity of MCVs in front of and behind the macula is denoted in red frames, while every image denoted by blue frames represents the average intensity of 10 MCVs.

follow-up of macula diseases). Therefore, the proposed method is anticipated to be neutral to the type of macula disease. This can be considered another contribution to the robustness of our method. A prospective clinical trial is needed to sustain these expectations of success. However, the physicians also reported that a common OCTA artifact is still present in the MCVs. The shadow of large blood vessels at ILM appears as black vessels at deep MCVs. The elimination of this artifact also needs to be addressed in future research. Experimenting on a local dataset is another future research.

The vessels' tortuosity (τ), which is one of the OCTA metrics [40], [41], can be calculated from the MCVs, as seen in Figure 7. This chart (Fig. 7) shows different amounts of "τ" at different depths. It can be noticed that there is a "general" gradual increase in "τ" as the MCVs cross the macula, then it is followed by a "general" gradual decrease in "τ" as the MCVs leave the macula region. This remark addresses the fact that the curvature shape of the macula should make each 5µm MCV contain only *partial* amounts of the macula vasculature. While this would permit perceiving the blood vessels network in sequential 5µm depths (as explained in previous paragraphs), it could also permit calculating the

OCTA metrics at sequential 5µm depths. This is a *futuristic advantage* of the MCVs. However, the calculated "τ" values are higher than the tortuosity indexes reported in reference [41], though the same method was used (equation 5). This can be attributed to many technical factors. The first, but the major reason, is the fact that in reference [41] the "τ" was calculated from projections of tens of µm thicknesses in the macula such as those in Fig. 1. In such case, the OCTA projections would have more number of vessels than each 5µm MCV would have. Once there is a high number of vessels in the OCTA image, the vessels would become intersected and overlapped which in such cases would shorten both the calculated vessels' lengths and the vessels' Euclidian distances in equation 5. Thus, a small value of "τ" would result. In contrast, a higher "τ" value would result from some 5µm MCVs due to the *uninterested* elongated blood vessels that are displayed according to coronal views entering and leaving the macula circular shape. Another major factor is the fact that the calculated "τ" values in Fig. 7 imply both the variety of disease severities in the 20 subjects (Normal and Abnormal OCTA subjects) and the two possible FOVs (3M and 6M OCTA scans from OptoVue OCTA machine), as seen

Enhanced Blood Vessels in OCTA Macula Coronal Views (MCV)
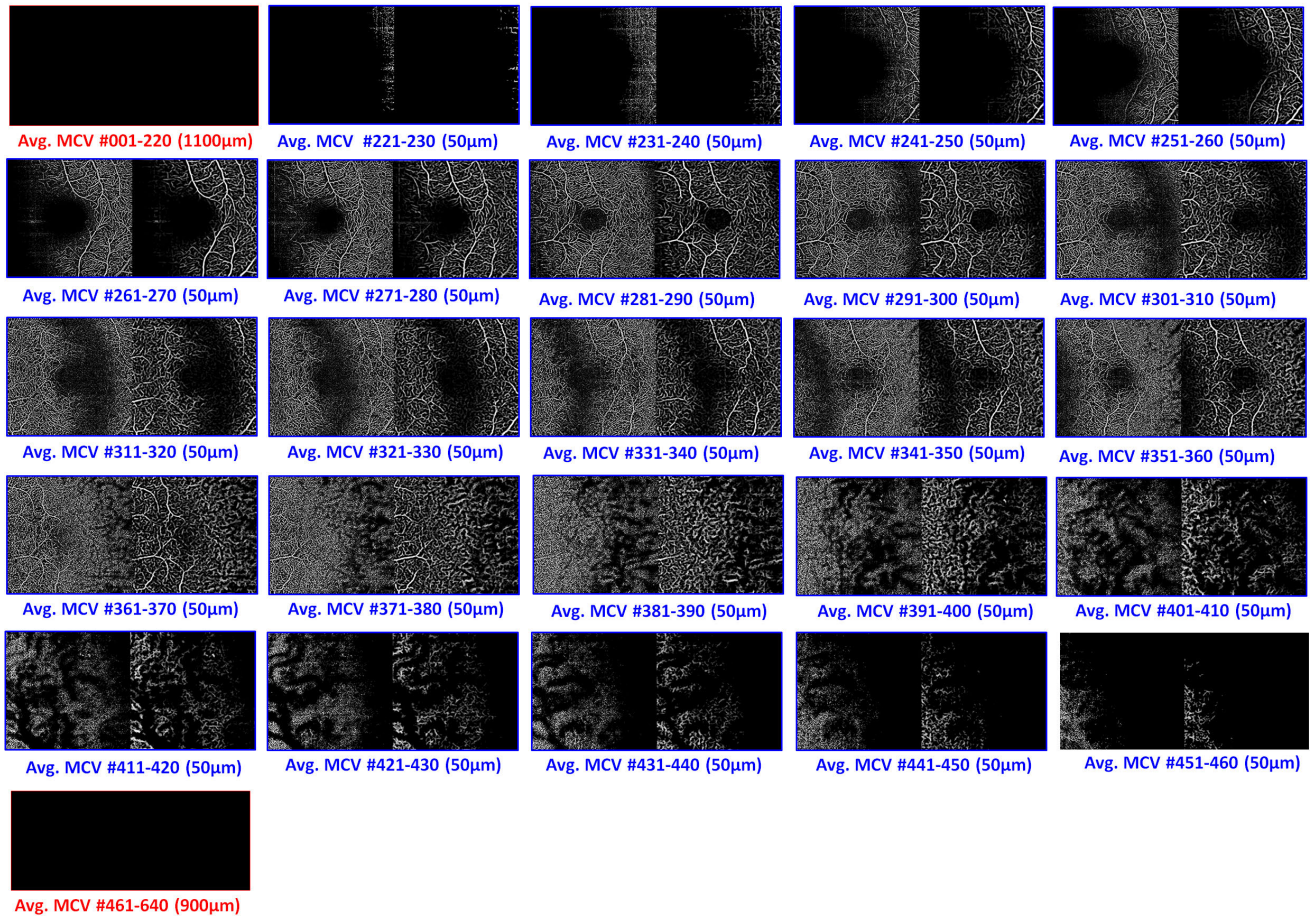

FIGURE 9. The projections of average MCVs of OCTA B-scan after applying Step-3-. The average intensity of enhanced MCVs in front of and behind the macula is denoted in red frames, while every image denoted by blue frames represents the average intensity of 10 enhanced MCVs.

in the Excel supplement file. In contrast, in reference [41], the authors utilized the ROSE dataset that contains only healthy control and Alzheimer's disease group [53]. Also, the subjects are all obtained from OptoVue and Heidelberg OCTA machines utilizing only the 3M FOV scan. The blood vessels would appear larger in the 6M FOV, resulting in larger "τ" values. The final technical factor, but with a marginal effect that we expect, is the image binarization method that could impact calculating the tortuosity index of any OCTA image.

Other OCTA metrics were reported in the literature, such as the vessel or perfusion density, vessel area density, and skeletonized vessel density or vessel length index [19], [20], [41], [42], [43], [45]. They were evaluated to assess the integrity (i.e. normal) or the disruption (i.e. abnormal) of the macula vasculature, which is not the objective of this paper. Furthermore, they were calculated on *slabs of macula thicknesses encompassing tens of microns, not from the 5 μm MCVs*. Fig. 7 suggests that these OCTA metrics could be explored on the 5μm MCVs, but this would extend the paper and deviate it to other research problems. Additionally, the tortuosity index and the OCTA metrics could be derived from all the 5 μm MCVs
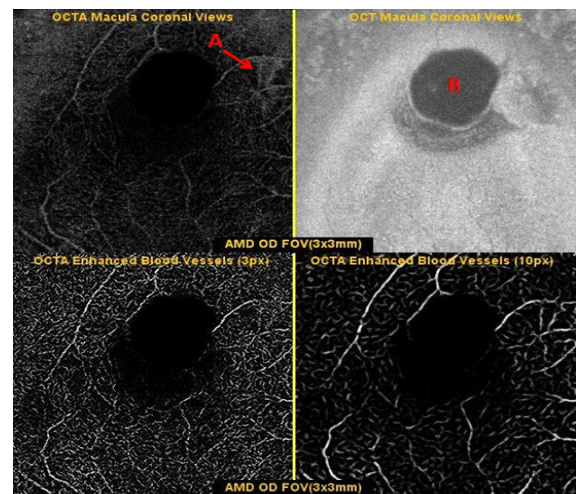

FIGURE 10. A Still-Frame from MCVs of AMD case showing two lesions. A: abnormal vascular configuration. B: Pigment Epithelial Detachment.

and then fed to an artificial intelligence scheme (e.g. deep learning or machine learning) to facilitate designing medical decision support systems similar to some papers in literature [21], [22], [23], [24], [46], [47], [48]. The evaluation
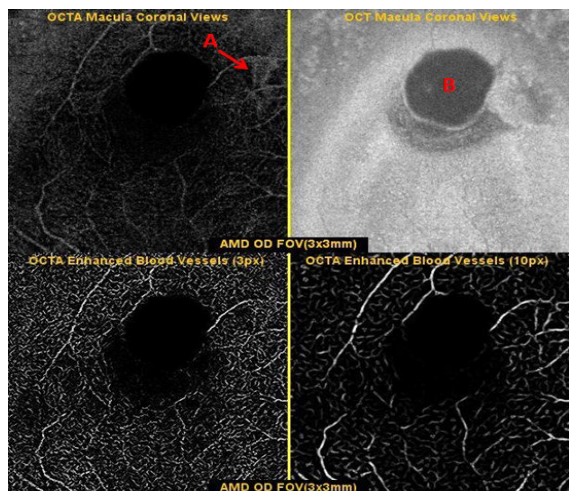
FIGURE 11. A Still-Frame from MCVs of OS AMD case showing choroidal Neovascular (CNV) Membrane.
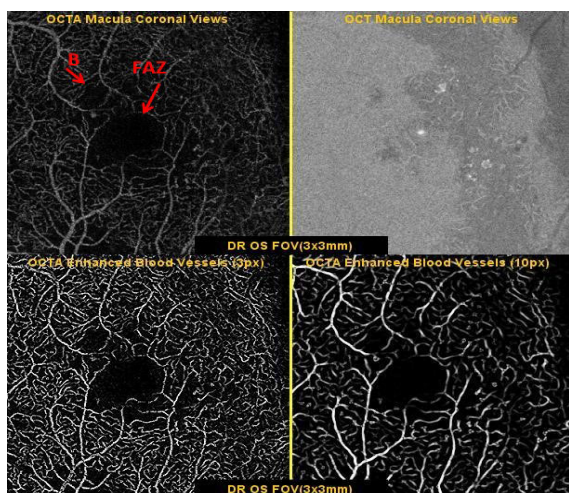

FIGURE 12. A Still-Frame from MCVs of OS DR case showing two lesions. Foveal Avascular Zone (FAZ) and focal area of loss of capillaries (B).

of calculating the OCTA metrics on all MCVs needs further separate research.

Finally, in the literature, there are reports assessing the impact of the 3D representation of macula blood vessels [25], [26], [27], [28], [29], [30], [49], [50], [51], [52]. These methods were based on surface and volumetric rendering [25], [28], [29], [30], [49], [50], [52] of the original 3D OCTA volume or they interpolated the 3D representation from 2D OCTA B-scans [26], [27], [51]. They succeeded in generating a 3D depiction of the macula's volume [25], [26], [27], [49], [50], [51], or they developed methods to generate a 3D shape model [28], map [29], [52], and surfacing the macula vasculature [30]. Similar to the OCTA quantitative metrics discussion in the preceding paragraph, the aim was to assess the 3D integrity or the disruption of the macula blood vessels. In contrast, this paper presents a method that should help ophthalmologists observe and identify *the orthogonal location and spread*, the axial and transversal diffusion, of the macula's normal and pathological conditions. The MCVs may participate successfully in the 3D

representation of the entire macula as in literature research [25], [28], [29], [30], [49], [50], [52], but this also needs a different research proposal.

In summary, the proposed CMIP procedures allow the *3D tracking of blood vessels* at all macula depths. The MCVs improve the monitoring of *the precise transversal and axial location and diffusion* of defects in the macula. This is expected to benefit the OCTA clinics to detect or follow up on macula disorders. The suggested scenario is to generate an animation of all 5μm sectional MCVs, similar to the displays in imaging other human organs. Thus, the ophthalmologists would observe the *orthogonal views of macula vasculature*. Based on the observational results, the 3D natural curvature of the macula and the series of coronal sections in all macula layers become visualized. The quantitative measure provides an indicator of the worthiness of the observational findings and anticipates the possibility of calculating other OCTA metrics from the 5μm MCVs. *Further research about the worthiness of the MCVs in OCTA clinics needs to be extended.*

VI. CONCLUSION

This experimental work proposes a novel CMIP method to solve the current challenges and limitations of OCTA displays. The proposed method generates coronal views from OCT and OCTA B-scans to allow the ophthalmologists to track the macula vasculature *3D diffusion at any macula spatial distance and axial depth*. Furthermore, the circular nature of the macula's oval-shaped becomes apparent, which allows viewing the 3D proliferation of macula vasculature. These two advantages could give physicians a comprehensive understanding of the 3D distribution of macula vasculature in OCT clinics. Additionally, the method uses a MATLAB function that successfully highlights the blood vessels at all macula depths, including deep layers. The experimental results have demonstrated that the method is robust and independent of the OCTA acquisition parameters, type of macula disorder, and the examined patient's OD or OS eye.

REFERENCES

[1] R. Weissleder and M. Nahrendorf, "Advancing biomedical imaging," *Proc. Nat. Acad. Sci. USA*, vol. 112, no. 47, pp. 14424–14428, Nov. 2015.

[2] A. M. Al-Hinnawi, B. O. Al-Naami, and H. Al-Azzam, "Collaboration between interactive three-dimensional visualization and computer aided detection of pulmonary embolism on computed tomography pulmonary angiography views," *Radiol. Phys. Technol.*, vol. 11, no. 1, pp. 61–72, 2018.

[3] B. Huang, Y. Ye, Z. Xu, Z. Cai, Y. He, Z. Zhong, L. Liu, X. Chen, H. Chen, and B. Huang, "3D lightweight network for simultaneous registration and segmentation of organs-at-risk in CT images of head and neck cancer," *IEEE Trans. Med. Imag.*, vol. 41, no. 4, pp. 951–964, Apr. 2022.

[4] A. S. Panayides, A. Amini, N. D. Filipovic, A. Sharma, S. A. Tsaftaris, A. Young, D. Foran, N. Do, S. Golemati, T. Kurc, K. Huang, K. S. Nikita, B. P. Veasey, M. Zervakis, J. H. Saltz, and C. S. Pattichis, "AI in medical imaging informatics: Current challenges and future directions," *IEEE J. Biomed. Health Informat.*, vol. 24, no. 7, pp. 1837–1857, Jul. 2020.

[5] H. Song, J. Lee, T. J. Kim, K. H. Lee, B. Kim, and J. Seo, "GazeDx: Interactive visual analytics framework for comparative gaze analysis with volumetric medical images," *IEEE Trans. Vis. Comput. Graph.*, vol. 23, no. 1, pp. 311–320, Jan. 2017.

[6] B. V. Bui, L. E. Downie, and R. G. Lindsay, "Optical coherence tomography: Seeing the unseen," *Clin. Exp. Exp.*, vol. 102, no. 3, pp. 193–194, May 2019.

[7] A. G. Podoleanu, "Optical coherence tomography," *J. Microsc.*, vol. 247, no. 3, pp. 209–219, Sep. 2012.

[8] J. B. Jonas, R. R. A. Bourne, R. A. White, S. R. Flaxman, B. A. J. Keeffe, J. Leasher, K. Naidoo, K. Pesudovs, T. Y. Wong, S. Resnikoff, and H. R. Taylor, "Visual impairment and blindness due to macular diseases globally: A systematic review and meta-analysis," *Amer. J. Ophthalmol.*, vol. 158, no. 4, pp. 808–815, Oct. 2014.

[9] W. L. Wong, X. Su, X. Li, C. M. G. Cheung, R. Klein, C.-Y. Cheng, and T. Y. Wong, "Global prevalence of age-related macular degeneration and disease burden projection for 2020 and 2040: A systematic review and meta-analysis," *Lancet Global Health*, vol. 2, no. 2, pp. e106–e116, Feb. 2014.

[10] M. Zhou, P.-C. Duan, J.-H. Liang, X.-F. Zhang, and C.-W. Pan, "Geographic distributions of age-related macular degeneration incidence: A systematic review and meta-analysis," *Brit. J. Ophthalmol.*, vol. 105, no. 10, pp. 1427–1434, 2021.

[11] D. K. Ferrara, N. Waheed, and J. S. Duker, "Investigating the choriocapillaris and choroidal vasculature with new optical coherence tomography technologies," *Prog. Retinal Eye Res.*, vol. 52, pp. 130–155, May 2016.

[12] A. H. Kashani, C.-L. Chen, J. K. Gahm, F. Zheng, G. M. Richter, P. J. Rosenfeld, Y. Shi, and R. K. Wang, "Optical coherence tomography angiography: A comprehensive review of current methods and clinical applications," *Prog. Retinal Eye Res.*, vol. 60, pp. 66–100, Sep. 2017.

[13] A. J. Augustin and J. Atorf, "The value of optical coherence tomography angiography (OCT-A) in neurological diseases," *Diagnostics*, vol. 12, no. 2, pp. 1–10, 2022.

[14] R. F. Spaide, J. M. Klancnik, and M. J. Cooney, "Retinal vascular layers imaged by fluorescein angiography and optical coherence tomography angiograph," *JAMA Ophthalmol.*, vol. 133, no. 1, pp. 45–50, 2015.

[15] R. F. Spaide, J. G. Fujimoto, N. K. Waheed, S. R. Sadda, and G. Staurenghi, "Optical coherence tomography angiography," *Prog. Retin. Eye Res.*, vol. 64, no. 9, pp. 1–55, May 2018.

[16] R. D. Laiginhas, D. Cabral, and M. Falcao, "Evaluation of the different thresholding strategies for quantifying choriocapillaris using optical coherence tomography angiography," *Quantum Imag. Med. Surg.*, vol. 10, no. 10, pp. 1994–2005, 2020.

[17] N. Mehta, P. X. Braun, I. Gendelman, A. Y. Alibhai, M. Arya, J. S. Duker, and N. K. Waheed, "Repeatability of binarization thresholding methods for optical coherence tomography angiography image quantification," *Sci. Rep.*, vol. 10, no. 1, p. 15368, 2020.

[18] J. H. Terheyden, M. W. M. Wintergerst, P. Falahat, M. Berger, F. G. Holz, and R. P. Finger, "Automated thresholding algorithms outperform manual thresholding in macular optical coherence tomography angiography image analysis," *PLoS One*, vol. 15, no. 3, Sep. 2020, Art. no. e0230260.

[19] A. Rabiolo, F. Gelormini, R. Sacconi, M. V. Cicinelli, G. Triolo, P. Bettin, K. Nouri-Mahdavi, F. Bandello, and G. Querques, "Comparison of methods to quantify macular and peripapillary vessel density in optical coherence tomography angiography," *PLoS One*, vol. 13, no. 10, Oct. 2018, Art. no. e0205773.

[20] W. Wei, Q. Zhang, S. G. Rayner, W. Qin, Y. Cheng, F. Wang, Y. Zheng, and R. K. Wang, "Automated vessel diameter quantification and vessel tracing for OCT angiography," *J. Biophotonics*, vol. 13, no. 12, 2020, Art. no. e202000248.

[21] M. Guo, M. Zhao, A. M. Y. Cheong, F. Corvi, X. Chen, S. Chen, Y. Zhou, and A. K. C. Lam, "Can deep learning improve the automatic segmentation of deep foveal avascular zone in optical coherence tomography angiography?" *Biomed. Sig. Process. Control*, vol. 66, Apr. 2021, Art. no. 102456.

[22] M. Guo, M. Zhao, A. M. Y. Cheong, H. Dai, A. K. C. Lam, and Y. Zhou, "Automatic quantification of superficial foveal avascular zone in optical coherence tomography angiography implemented with deep learning," *Vis. Comput. Ind., Biomed., Art*, vol. 2, no. 1, p. 21, 2019.

[23] J. Lo, M. Heisler, V. Vanzan, S. Karst, I. Z. Matovinovic, S. Loncaric, E. V. Navajas, M. F. Beg, and M. V. Šarunic, "Microvasculature segmentation and intercapillary area quantification of the deep vascular complex using transfer learning," *Transl. Vis. Sci. Technol.*, vol. 9, vol. 2, p. 38, Jul. 2020.

[24] Z. Liu, C. Wang, X. Cai, H. Jiang, and J. Wang, "Discrimination of diabetic retinopathy from optical coherence tomography angiography images using machine learning methods," *IEEE Access*, vol. 9, pp. 51649–51689, 2021.

[25] S. Fragiotta, C. Ciancimino, A. Perdicchi, A. De Paula, S. Abdolrahimzadeh, and G. Scuderi, "Volume rendering of angiographic optical coherence tomography angiography in fovea plana and normal foveal pit," *Frontiers Neurol.*, vol. 12, Apr. 2021, Art. no. 633492.

[26] S. Yu, J. Xie, J. Hao, Y. Zheng, J. Zhang, Y. Hu, J. Liu, and Y. Zhao, "3D vessel reconstruction in OCT-angiography via depth map estimation," in *Proc. IEEE 18th Int. Symp. Biomed. Imag. (ISBI)*, Nice, France, Jul. 2021, pp. 1609–1613, doi: 10.1109/ISBI48211.2021.9434042.

[27] Y. Ji, K. Zhou, S. H. Ibbotson, R. K. Wang, C. Li, and Z. Huang, "A novel automatic 3D stitching algorithm for optical coherence tomography angiography and its application in dermatology," *J. Biophoton.*, vol. 14, no. 11, Jul. 2021, Art. no. e202100152.

[28] J. Zhang, Y. Qiao, M. S. Sarabi, M. M. Khansari, J. K. Gahm, A. H. Kashani, and Y. Shi, "3D shape modeling and analysis of retinal microvasculature in OCT-angiography images," *IEEE Trans. Med. Imag.*, vol. 39, no. 5, pp. 1335–1346, May 2020.

[29] M. S. Sarabi, M. M. Khansari, J. Zhang, S. Kushner-Lenhoff, J. K. Gahm, Y. Qiao, A. H. Kashani, and Y. Shi, "3D retinal vessel density mapping with OCT-angiography," *IEEE J. Biomed. Health Informat.*, vol. 24, no. 12, pp. 3466–3479, Dec. 2020.

[30] P. M. Maloca, S. Feu-Basilio, J. Schottenhamml, P. Valmaggia, H. P. N. Scholl, J. Rosinés-Fonoll, S. Marin-Martinez, N. Inglin, M. Reich, C. Lange, C. Egan, S. Zweifel, A. Tufail, R. F. Spaide, and J. Zarranz-Ventura, "Reference database of total retinal vessel surface area derived from volume-rendered optical coherence tomography angiography," *Sci. Rep.*, vol. 12, no. 1, p. 3695, 2022.

[31] A. R. Al-Hinnawi, "Reconstruction and visualization of 5μm sectional coronal views for macula vasculature in OCTA," IEEE Dataprot, USA, Jun. 2022, doi: 10.21227/gx1z-tj11.

[32] M. Li, Y. Zhang, Z. Ji, K. Xie, S. Yuan, Q. Liu, and Q. Chen, "IPN-V2 and OCTA-500: Methodology and dataset for retinal image segmentation," 2020, *arXiv:2012.07261*.

[33] M. Li, Y. Chen, Z. Ji, K. Xie, S. Yuan, Q. Chen, and S. Li, "Image projection network: 3D to 2D image segmentation in OCTA images," *IEEE Trans. Med. Imag.*, vol. 39, no. 11, pp. 3343–3354, Nov. 2020.

[34] A. F. Frangi, W. J. Niessen, K. L. Vincken, and M. A. Viergever, "Multiscale vessel enhancement filtering," in *Proc. Int. Conf. Med. Image Comput. Comput.-Assist. Intervent.*, 1998, pp. 130–137.

[35] T. Jerman, F. Pernuš, B. Likar, and Ž. Špiclin, "Enhancement of vascular structures in 3D and 2D angiographic images," *IEEE Trans. Med. Imag.*, vol. 35, no. 9, pp. 2107–2118, Sep. 2016.

[36] A. M. Al-Hinnawi, B. O. Al-Naami, and M. M. Al-Latayfeh, "Optic nerve head slope-based quantitative parameters for identifying open-angle glaucoma on SPECTRALIS OCT images," *Int. Ophthalmol.*, vol. 37, no. 4, pp. 979–988, 2017.

[37] A. M. Al-Hinnawi, A. M. Alqasem, and B. O. Al-Naami, "Three-dimensional surface presentation of optic nerve head from SPECTRALIS OCT images: Observing glaucoma patients," *Int. Ophthalmol*, vol. 39, no. 9, pp. 1939–1947, 2019.

[38] A. M. Al-Hinnawi, A. Al-Bashir, and A. M. Alqasem, "New computerized volume measurement method for optic nerve head (ONH) region comparison with measurements by Heidelberg SPECTRALIS optical coherence tomography," *Informat. Med. Unlocked*, vol. 20, Jun. 2020, Art. no. 100383.

[39] A. Ishibazawa and N. Waheed. *Which OCTA Machine Should You Get? Pros and Cons of Each System*, Retina Round Up. Accessed: Jan. 28, 2019. [Online]. Available: https://retinaroundup.com/2019/01/28/which-octa-machine-should-you-get-pros-and-cons-of-each-system/

[40] J. F. Bille, *High Resolution Imaging in Microscopy and Ophthalmology: New Frontiers in Biomedical Optics*. Switzerland: Cham, Switzerland: Springer, 2019, pp. 59–87 and 135-160, doi: 10.1007/978-3-030-16638-0.

[41] F. Martilli and C. Giacomozzi, "Tortuosity index calculations in retinal images: Some criticalities arising from commonly used approaches," *Information*, vol. 12, no. 11, p. 466, 2021.

[42] Z. Chu, J. Lin, C. Gao, C. Xin, Q. Zhang, C. C. L. Roisman, G. Gregori, P. J. Rosenfeld, and R. K. Wang, "Quantitative assessment of the retinal microvasculature using optical coherence tomography angiography," *J. Biomed. Opt.*, vol. 21, no. 6, p. 66008, 2016.

[43] V. Pramil, E. Levine, and N. Waheed, "Macular vessel density in diabetic retinopathy patients: How can we accurately measure and what can it tell us?" *Clin. Ophthalmol.*, vol. 15, pp. 1517–1527, Apr. 2021.

[44] Q. S. You, J. C. H. Chan, A. L. K. Ng, B. K. N. Choy, K. C. Shih, J. J. C. Cheung, J. K. W. Wong, J. W. H. Shum, M. Y. Ni, J. S. M. Lai, G. M. Leung, C. M. G. Cheung, T. Y. Wong, and I. Y. H. Wong, "Macular vessel density measured with optical coherence tomography angiography and its associations in a large population-based study," *Invest. Ophthalmol. Vis. Sci.*, vol. 60, no. 14, pp. 4830–4837, 2019.

[45] K. K. Cheng, B. L. Tan, L. Brown, C. Gray, E. Bianchi, B. Dhillon, T. MacGillivray, and A. J. Tatham, "Macular vessel density, branching complexity and foveal avascular zone size in normal tension glaucoma," *Sci. Rep.*, vol. 11, p. 1056, Jan. 2021.

[46] S. M. Zekavat, V. K. Raghu, M. Trinder, Y. Ye, S. Koyama, M. C. Honigberg, Z. Yu, A. Pampana, S. Urbut, S. Haidermota, D. P. O'Regan, H. Zhao, P. T. Ellinor, A. V. Segrè, T. Elze, J. L. Wiggs, J. Martone, R. A. Adelman, N. Zebardast, L. Del Priore, J. C. Wang, and P. Natarajan, "Deep learning of the retina enables phenome- and genome-wide analyses of the microvasculature," *Circulation*, vol. 145, no. 2, pp. 134–150, Jan. 2022.

[47] D. Le, T. Son, and X. Yao, "Machine learning in optical coherence tomography angiography," *Exp. Biol. Med.*, vol. 246, no. 20, pp. 2170–2183, Oct. 2021.

[48] O. O. Sule, "A survey of deep learning for retinal blood vessel segmentation methods: Taxonomy, trends, challenges and future directions," *IEEE Access*, vol. 10, pp. 38202–38236, 2022.

[49] E. Borrelli, R. Sacconi, G. Klose, L. de Sisternes, F. Bandello, and G. Querques, "Rotational three-dimensional OCTA: A notable new imaging tool to characterize type 3 macular neovascularization," *Sci. Rep.*, vol. 9, p. 7053, Nov. 2019.

[50] J. S. Agranat, J. B. Miller, V. P. Douglas, K. A. A. Douglas, A. Marmalidou, M. A. Cunningham, and S. K. Houston, "The scope of three-dimensional digital visualization systems in vitreoretinal surgery," *Clin. Ophthalmol.*, vol. 24, no. 13, pp. 2093–2096, 2019.

[51] A. Athwal, C. Balaratnasingam, D. Yu, M. Heisler, M. V. Sarunic, and M. J. Ju, "Optimizing 3D retinal vasculature imaging in diabetic retinopathy using registration and averaging of OCT-A," *Biomed. Opt. Exp.*, vol. 12, no. 1, pp. 553–570, 2021.

[52] F. A. Bartol-Puyal, C. Isanta, P. Calvo, S. Méndez-Martínez, Ó. Ruiz-Moreno, and L. Pablo, "Mapping of choriocapillaris vascular density in young and aged healthy subjects," *Eur. J. Ophthalmol.*, vol. 32, no. 5, pp. 2789–2800, 2022.

[53] Y. Ma, H. Hao, J. Xie, H. Fu, J. Zhang, J. Yang, Z. Wang, J. Liu, Y. Zheng, and Y. Zhao, "ROSE: A retinal OCT-angiography vessel segmentation dataset and new model," *IEEE Trans. Med. Imag.*, vol. 40, no. 3, pp. 928–939, Mar. 2021.

AHMED BANIMUSTAFA (Senior Member, IEEE) received the M.Sc. degree from UWE, Bristol University, and the Ph.D. degree from Aberystwyth University, U.K., with a prestigious scholarship from the Computer Science Department. He previously worked with the American University of Madaba, Aberystwyth University, Philadelphia University, the Jordan University of Science and Technology, and Motorola Mobility (Acquired later by Google LLC). He is an Assistant Professor of data science and artificial intelligence with ISRA University, Jordan. His major research interests include machine learning, data science, software engineering, and health informatics. He is currently a member of the IEEE Computer Society, the IEEE Computational Intelligence Society, and the IEEE Robotics and Automation Society.

MOTASEM AL-LATAYFEH is currently an Associate Professor of medicine with the Department of General and Special Surgery, Hashemite University. He is a member of the Jordan Consultant Ophthalmologists and an Eye Surgery Specialist with Prince Hamza Hospital, Amman, Jordan.

MITRA TAVAKOLI received the B.Sc. degree (Hons.) in optometry from the Mashad University of Medical Sciences, in 2000, the M.Sc. degree in optometry from the University of Bradford, in 2003, and the Ph.D. degree in medicine from the School of Medicine, University of Manchester, in 2008. She is currently an Associate Professor of medicine with the University of Exeter and is distinguished for her significant contribution to our understanding of small fiber neuropathy in diabetes and establishing the technique of "Corneal Confocal Microscopy." Her recent work elucidated the role of intervention for the regeneration of nerves in type 1 and type 2 diabetes. Her earlier work showed for the first time that CCM could be used to quantify early small nerve fiber damage with good sensitivity and specificity. Her ongoing research into understanding the role of novel intervention in rare models of neuropathies initiated a new direction of research. In addition, she is widely respected for training scientists across the world. She spearheads new technologies and contributes to major U.K. and international collaborations. She was a member of the College of Optometrists (MCOptom), in 2016. She received the 2019 Fellowship Higher Education Academy (FHEA), the 2010 Fellowship American Academy of Optometry (FAAO), and the 2009 Fellowship British Contact Lens Association (FBCLA).

ABDEL-RAZZAK M. AL-HINNAWI was born in Damascus, Syria, in 1968. He received the B.S. degree in biomedical engineering from Damascus University, in 1991, and the M.Sc. and Ph.D. degrees in medical imaging science from the University of Aberdeen, U.K., in 1995 and 1999, respectively. Since 1999, he has been working as an Assistant and Associate Professor with the biomedical engineering and medical imaging department at universities in Jordan and Syria. He is currently an Associate Professor with Isra University, Jordan. He has authored several Scopus- /ISI-indexed articles and one e-chapter. His research interests include quantitative analysis of medical images and 3-D visualization and biomedical engineering and medical devices.

• • •